Received: 29 March 2022 | Revised: 11 May 2022 | Accepted: 4 June 2022

DOI: 10.1002/hyp.14633

RESEARCH ARTICLE

WILEY

Response of runoff components to climate change in the source-region of the Yellow River on the Tibetan plateau

Ting Zhang | **Dongfeng Li** | **Xixi Lu**

Department of Geography, National University of Singapore, Kent Ridge, Singapore

Correspondence
Dongfeng Li, Department of Geography, National University of Singapore, Kent Ridge 117570, Singapore.
Email: dongfeng@u.nus.edu

Funding information
Ministry of Education - Singapore; Ministry of Education

Abstract

Climate change will likely increase the total streamflow in most headwaters on the Tibetan Plateau in the next decades, yet the response of runoff components to climate change and permafrost thaw remain largely uncertain. Here, we investigate the changes in runoff components under a changing climate, based on a high-resolution cryosphere-hydrology model (Spatial Processes in Hydrology model, SPHY) and multi-decadal streamflow observations at the upstream (Jimai) and downstream stations (Maqu and Tangnaihai) in the source-region of the Yellow River (SYR). We find that rainfall flow dominates the runoff regime in SYR (contributions of 48%–56%), followed by snowmelt flow (contributions of 26%/23% at Maqu/Tangnaihai). Baseflow is more important at Jimai (32%) than at the the downstream stations (21%–23%). Glacier meltwater from the Anyê Maqên and Bayankala Mountains contributes negligibly to the downstream total runoff. With increasing temperature and precipitation, the increase in total runoff is smaller in the warm and wet downstream stations than in the cold and dry upstream station. This is because of a higher increase in evapotranspiration and a larger reduction in snowmelt flow in the downstream region in response to a warming climate. With temperature increase, there is less increase in rainfall flow in the downstream region due to increased water loss through evapotranspiration. Meanwhile, the decline in snowmelt flow is larger further downstream, which can negatively impact the spring irrigation for the whole Yellow River basin that supports the livelihoods of 140 million people. Importantly, we find that baseflow plays an increasingly important role in the permafrost-dominated upstream region with atmospheric warming and permafrost thaw, accompanied by decreased surface flow. These findings improve our current understanding of how different hydrological processes respond to climate change and provide insights for optimizing hydropower and irrigation systems in the entire Yellow River basin under a rapidly changing climate.

KEYWORDS
climate change, permafrost thaw, response mechanism, runoff components, source-region of Yellow River

Novelty statement

The source-region of the Yellow River (SYR) on the Tibetan Plateau is the "water tower" of the Yellow River. However, prior studies in SYR mainly focused on changes in total runoff, instead of responses of different runoff components to climate change. In this study, we separated the runoff components in SYR, simulated their responses to climate change, and discussed the impact of permafrost thaw on baseflow. This study highlights the increasingly important role of permafrost thaw on hydrological processes in a warming Tibetan Plateau. In permafrost-dominated regions, runoff regime will likely transition from a surface-water-dominated system towards a groundwater-dominated system.

1 | INTRODUCTION

The Yellow River, China's mother river, supports the freshwater supply for 140 million people and 13% of China's agricultural land (Cai & Rosegrant, 2004; Yue et al., 2017). The source-region of the Yellow River (SYR) on the Tibetan Plateau is deemed as the "water tower" of the Yellow River (Immerzeel et al., 2010; Yuan et al., 2018) because it contributes 55%–70% of the annual runoff in the entire Yellow River with a drainage area fraction of only 16% (121 790 km^2) (Table S1) (Zhou & Huang, 2012). The recent amplified climate change on the Tibetan Plateau has accelerated glacier-snow-permafrost degradation and impacted the hydrological processes in many headwater regions (Immerzeel et al., 2020; Li et al., 2020; Li et al., 2021; Wang et al., 2021), triggering significant social and economic uncertainties to the downstream regions (Duan et al., 2020; Pritchard, 2019; Zheng et al., 2009). Thus, understanding how streamflow in SYR, particularly various runoff components (e.g., glacier-melt flow, snowmelt flow, rainfall flow, and baseflow), respond to climate change has important implications for future water resource management in the entire Yellow River.

Prior studies on streamflow in SYR have mostly focused on the response of total runoff to climate change (Jin et al., 2018; Lan et al., 2010; Zheng et al., 2009). For instance, the reduced total runoff after the 1990s has been attributed to increased temperature, enhanced evapotranspiration, and decreased precipitation either based on statistical models (Hu, Maskey, Uhlenbrook, & Zhao, 2011; Lan et al., 2010; Zhou & Huang, 2012), simple water balance models (Taihua Wang, Yang, Yang, et al., 2018; Zheng et al., 2018), or large-scale hydrological models (Meng et al., 2016). However, the response of different runoff components to climate change remains less investigated (Immerzeel et al., 2013; Khanal et al., 2021). The impact of climate change is complex for cryosphere basins, especially for a basin underlain by permafrost and seasonally frozen ground like SYR (Cuo et al., 2013; Immerzeel et al., 2010). For instance, as the climate warms, the contribution of snowmelt to the total flow may either decrease due to a shift of snowfall to rainfall (Qin et al., 2020) or increase due to snowpack melting (Duan et al., 2017). The response of baseflow to climate warming is complicated by the hydrological impacts of permafrost degradation (Walvoord & Kurylyk, 2016). Permafrost thaw can alter the relative contributions of surface flow and baseflow, and then affect the streamflow seasonality (Ma et al., 2019).

Compared with statistical methods and conventional rainfall-runoff models (Hu, Maskey, Uhlenbrook, et al., 2011; Lan et al., 2010; Zhou & Huang, 2012), physics-based fully-distributed hydrological models involving cryospheric processes are more powerful in separating runoff components and investigating their responses to climate change in cryosphere basins at finer spatial–temporal scales (Lutz et al., 2014; Tiel et al., 2020). The Spatial Processes in Hydrology (SPHY) model is a high-resolution fully-distributed cryosphere-hydrology model incorporating cryospheric processes of glacier melt and snowmelt (Terink et al., 2015; Tiel et al., 2020). SPHY has been widely used among the hydrological community and has shown overall satisfactory performance in the world's 78 mountain water towers (Immerzeel et al., 2020), but its performance in SYR has not been robustly tested due to the lack of in-situ observed runoff (Khanal et al., 2021). In this study, SPHY is selected to uncover the various runoff generation processes in SYR together with the historical runoff observations at three stations and examine the responses of runoff components to climate change.

The three objectives of this study are: (1) to quantify the contributions of runoff components (e.g., glacier-melt flow, snowmelt flow, rainfall flow, and baseflow) to the total runoff at a monthly scale in SYR; (2) to examine the responses of different runoff components to climate change; (3) to discuss the impact of permafrost thaw on baseflow. The results will improve our understanding of the hydrological processes and response mechanism of runoff components to future climate change on the Tibetan Plateau. It also has significant implications for estimating seasonal freshwater supply in SYR and its downstream region in a changing climate.

2 | STUDY AREA AND MATERIALS

2.1 | Study area

In this study, the source-region of the Yellow River (SYR) is defined as the catchment above the Tangnaihai Hydrological Station, between 95°50′–103°30′E and 32°20′–36°10′N (Figure 1a). Hydrological data in SYR was observed at three stations. The upstream station covers the region above Jimai (45 850 km^2), and the two downstream stations cover the region above Maqu (86 748 km^2) and the region above Tangnaihai (121 790 km^2), respectively.

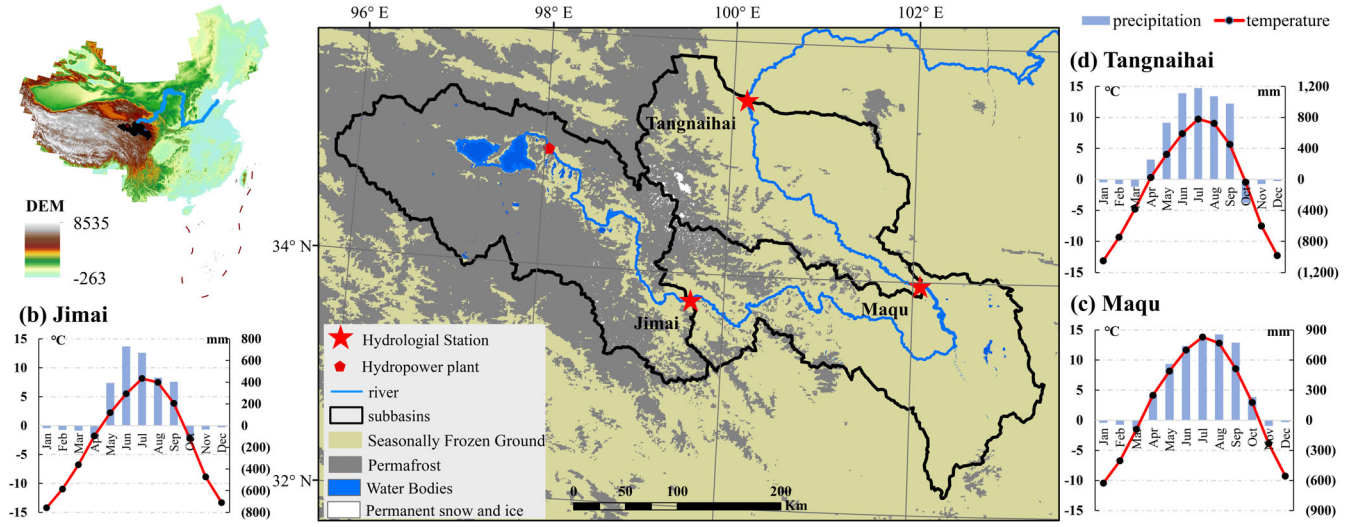

FIGURE 1 Basic land cover and climate characteristics in the source-region of Yellow River (SYR). There are three stations in SYR (the upstream station: Jimai; the downstream stations: Maqu and Tangnaihai). The monthly average temperature (red lines) and monthly precipitation (blue bars) in SYR are shown in (b) Jimai, (c) Maqu, (d) Tangnaihai

TABLE 1 Statistics of land use in SYR

Land use types	Cropland	Forest	Grassland	Bare ground	Permanent snow and glacier	Water bodies
Area in SYR (km^2)	48 349.4	872 186.9	9 161 226.5	1 355 522.7	16 016.6	726 233.8
Area % at three stations in SYR						
Above Jimai	1.02	1.83	74.43	17.38	0.34	5.00
Above Maqu	0.50	4.72	77.11	9.84	0.06	0.17
Above Tangnaihai (SYR)	0.40	7.16	75.22	11.13	0.13	5.96

The terrain varies greatly in SYR, with elevation increasing from west to east, ranging from 6184 meters above sea level (m a.s.l.) to 2689 m a.s.l. Permafrost and seasonally frozen ground are widely distributed in SYR and 84% of the area in the upstream region of Jimai is covered by permafrost (Figure 1a). The main type of land cover is grassland (75.22%), followed by bare ground and forest (Table 1). Main vegetation types include alpine meadow, steppe, and sparse vegetation (Qin et al., 2017). Only about 0.4% of SYR is covered by permanent snow and glacier, which are concentrated in the Anyê Maqên and Bayankala Mountains. There are two large lakes in the research region, namely Ngoring and Gyaring, above Jimai.

SYR has an alpine continental climate (Song et al., 2009). From 2000 to 2015, the annual average temperature among three stations ranged from 2.52 to −4.35°C, with the highest temperature at Maqu and the lowest temperature at Jimai (Figure 1b–d). Annual precipitation from upstream to downstream increased from 160 to 700 mm (Figure S1a). Rainfall flow and snowmelt flow are the main contributors to runoff in SYR (Meng et al., 2016). Rainfall is confined from June to August and snowfall generally begins in October (Figure 1b–d). Moreover, many studies have reported that the climate in SYR has become warmer and wetter since 2000 (Hu, Maskey, & Uhlenbrook, 2011; Jin et al., 2018). Following earlier studies (Wang et al., 2018) and the monthly average temperature and precipitation (Figure 1), the period between April and June is taken as spring; the period between July and September is taken as summer; the period between October and December is taken as autumn; the period between January and March is taken as winter. Furthermore, SYR is a relatively intact catchment and was barely affected by human interference before 2000 (Lu et al., 2018).

2.2 | Runoff observations and forcing data

Monthly streamflow observations from 1990 to 1999 and daily observations from 2000 to 2015 of three stations, namely Tangnaihai (location: 100.15E, 35.5 N), Maqu (location:102.08E, 33.97 N) and, Jimai (location:99.65 N, 33.77 N), were obtained from the Yellow River Conservancy Commission of the Ministry of Water Resources (http://www.yrcc.gov.cn/).

SPHY was driven by meteorological forcings (temperature and precipitation), with inputs of elevation, land cover, soil, and glacier coverage data. Elevation in SYR was derived from SRTM (Shuttle Radar Topography Mission) V4 and can be downloaded from the Resource and Environment Science and Data Center (http://www.resdc.cn/data), with a 250-m spatial resolution. Land cover in SYR was clipped from GlobCover Land Cover Map developed by the

European Space Agency (http://due.esrin.esa.int/page_globcover.php), which covers the period from December 2004 to June 2006 with a 300-m spatial resolution. Soil types were clipped from the China soil map (http://westdc.westgis.ac.cn/zh-hans/data/), with a 900-m spatial resolution which is based on the harmonized world soil database and the Nanjing Soil Research Institute at the second national Land Survey. Physical parameters of different soil types can be checked from the HiHydroSoil database (http://www.sphy.nl/) provided by FutureWater. Glacier coverage within SYR was derived from Randolph Glacier Inventory (RGI V6.0, https://www.glims.org/RGI/rgi60_dl.html); further information can be found at Pfeffer et al. (2014).

Historical (1990–2015) daily temperature (max, min, average) and precipitation were sourced from the China Meteorological Forcing Dataset (CMFD, https://data.tpdc.ac.cn/en/data/8028b944-daaa-4511-8769-965612652c49/) with a 0.1-degree spatial resolution and a 3-h temporal resolution. This dataset was developed by merging multiple sources with high accuracy and resolution, including in-situ observations from approximately 700 China Meteorological Administration stations, Tropical Rainfall Measuring Mission (TRMM) precipitation data, Global Energy and Water Exchanges-Surface Radiation Budget (GEWEX-SRB) radiation data, Global Land Data Assimilation System (GLDAS), and Princeton forcing data (He et al., 2020). Moreover, CMFD has been demonstrated to have good performance over Tibetan Plateau and has good capability in simulating the runoff at poorly gauged catchments (Huang et al., 2020; Yang et al., 2021).

3 | RUNOFF SIMULATION BASED ON A CRYOSPHERE-HYDROLOGICAL MODEL

The SPHY model ensures robust performance in cases of data scarcity and is a high-resolution grid-based model, which usually runs at a spatial resolution between 250 m and 1 km (Terink et al., 2015). SPHY also has merits over the commonly used models such as Soil and Water Assessment Tool (SWAT) or Variable Infiltration Capacity (VIC) in terms of input data requirement. For instance, it only needs precipitation and temperature data as climate forcing and does not require other climatic data such as wind speed and radiation (Lutz et al., 2014).

The soil water processes in SPHY are modelled at three soil layers, namely root layer, sub-layer, and groundwater layer. In this study, SPHY was used to simulate the runoff in SYR at a 500-m spatial resolution and daily time steps. According to the operating time of the Huangheyan hydropower plant, the monthly runoff observations from 1990 to 1999 were used to calibrate the hydrological model, and the observations from 2000 to 2015 were used for model validation at three stations. The model was warmed up from 1990 to 1993 to get the most reasonable initial state (Tiel et al., 2020) and the effective simulation began in 1994. There are six modules included in this study's simulation, namely snow, glacier, soil, groundwater, evapotranspiration, and routing module. The simulation processes of total runoff in SPHY are introduced below; the simulation of evapotranspiration and runoff components are introduced in Text S1. More information on SPHY can be found in Terink et al. (2015). The main calibrated parameters are listed in Table S2.

TABLE 2 SPHY evaluation at three stations in SYR

	Calibration			Verification		
	NSE	RE	*R*	NSE	RE	*R*
Jimai	0.70	−0.10	0.89	0.72	−0.01	0.85
Maqu	0.61	−0.23	0.84	0.71	−0.06	0.85
Tangnaihai	0.76	−0.09	0.88	0.74	0.06	0.88

Abbreviations: NSE, Nash-Sutcliffe efficiency; *R*, Pearson correlation coefficient; RE, relative error.

The model performance was evaluated based on three widely used indices: the Nash-Sutcliffe efficiency coefficient (NSE, 0–1) (Nash & Sutcliffe, 1970), Pearson correlation coefficient (*R*, 0–1), and relative error (RE). Smaller RE, larger NSE, and higher R indicate more accurate simulation. Notably, RE is defined as the sum of the difference between simulated and observed runoff divided by the sum of observed runoff in this study. From previous studies, the model with NSE over 0.5 and RE less than 25% can be taken as a satisfactory model (Foglia et al., 2009; Han et al., 2019; Moriasi et al., 2007; Zhang et al., 2008).

3.1 | Total runoff and routing

For each grid, the total runoff (*QTot*) is the sum of all runoff components, namely glacier-melt flow (*GRo*), snowmelt flow (*SRo*), rainfall flow (*RRo*), and baseflow (*BF*). Rainfall flow consists of surface flow (RO) and lateral flow (LF).

$$\begin{aligned} QTot &= GRo + SRo + RRo + BF \\ &= GRo + SRo + (RO + LF) + BF \end{aligned} \quad (1)$$

To estimate the river runoff, *QTot* needs to be routed along with the flow direction network. In SPHY, it is calculated as the accumulated amount of water flows out of the grid into its neighbouring downstream grids and considers the flow delay in a river basin by including a flow recession coefficient (*Kx*). *Kx* is related to the size and characteristics of the catchment. The higher *Kx* corresponds to a slower response of the catchment. The river runoff (Q_{rout}) is estimated by:

$$\begin{aligned} Q_{rout,t} &= (1 - Kx) \times Q_{accu,t} + Kx \times Q_{rout,t-1} \\ Q_{accu,t} &= \text{accuflux}(F_{dir}, QTot_t^*), \\ QTot_t^* &= \frac{QTot_t \times 0.001 \times A}{24 \times 3600}, \end{aligned} \quad (2)$$

where F_{dir} is the flow direction network. Q_{accu} the accumulated runoff on day *t* without considering the flow delay. *A* the basin area with a unit in m^2. QTot with a unit in millimetres per day (mm day^{-1}) is converted to *QTot** with a unit in m^3/s.

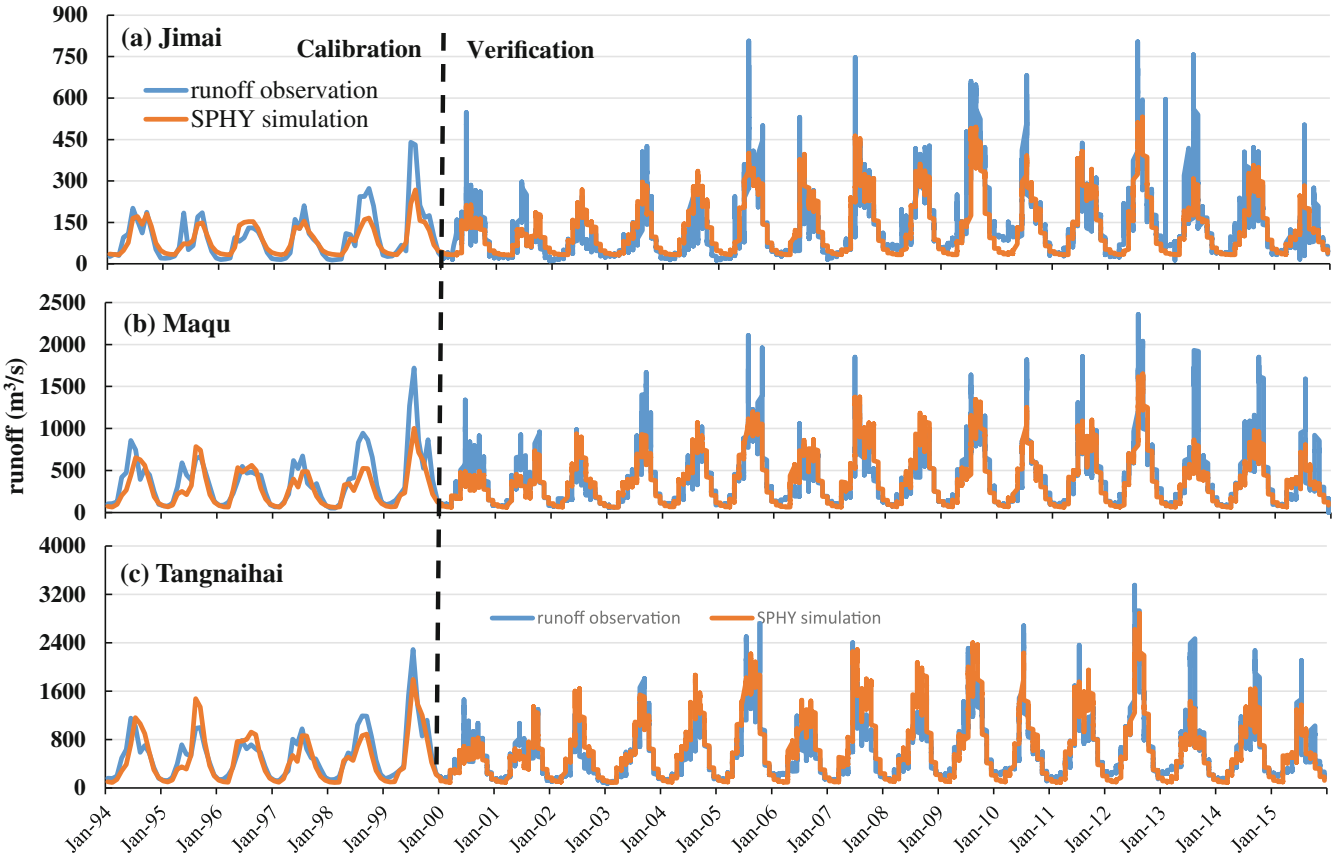

FIGURE 2 Comparison of monthly simulated and observed runoff in the calibration period from 1994 to 1999 (the left of the dotted line) and daily simulated and observed runoff in the verification period from 2000 to 2015 (the right of the dotted line) at (a) Jimai, (b) Maqu, and (c) Tangnaihai

3.2 | Runoff simulation in SYR

For the calibration period (from 1994 to 1999), NSEs exceeded 0.6 for all three stations in SYR, with a high R (0.84–0.89) (Table 2, Figure 2). The evaluation results indicate that the inter- and intra-annual variability of runoff can be well captured by SPHY. The runoff peaks among the three stations were underestimated with RE ranging from −9% to −23%, especially in 1998 and 1999. This may have resulted from the underestimation of rainfall peaks by CMFD for several years (Zhou et al., 2015). Generally, the calibrated parameters (Table S2) are suitable for the runoff simulation in SYR. During the validation period (from 2000 to 2015), the simulated runoff was generally commensurate with observed runoff at the daily scale for all three stations, with NSE over 0.70 and R ranging from 0.85 to 0.88. There is no significant underestimation or overestimation in the verification period (RE within ±6%). These metrics show that the SPHY model constructed in this study has a satisfactory performance in SYR.

4 | RESULTS

In this section, runoff components and their responses to climate perturbation are analysed. Hydrological responses are compared between the upstream station (Jimai) and the downstream stations (Maqu and Tangnaihai) according to the spatial heterogeneity in terrain, land cover, temperature, and precipitation (see Section 2.1).

4.1 | Current runoff components in SYR

The contributions of runoff components to the total runoff vary between upstream and downstream stations in SYR (Figure 3) and such spatial variation is clearer under the 500-m spatial resolution (Figure 4). For the entire SYR, rainfall flow accounts for the largest proportion of the total runoff, followed by snowmelt flow, baseflow, and glacier-melt flow, respectively (Figure 3c). The contributions of runoff components vary among three stations due to differences in terrain and climate characteristics. Specifically, the average elevation in the upstream region (4400 m a.s.l.) exceeds that in the downstream region (3900 m a.s.l.). Accordingly, the annual average temperature (lower than 0°C, Figure S2a) and annual precipitation are lower (Figure S1a) in the upstream region than in the downstream region. Such difference results in a colder and dryer climate at the upstream station, relative to the downstream stations.

The contribution of snowmelt flow to the total runoff is highest at Maqu (26%), followed by Tangnaihai (23%), and Jimai (20%)

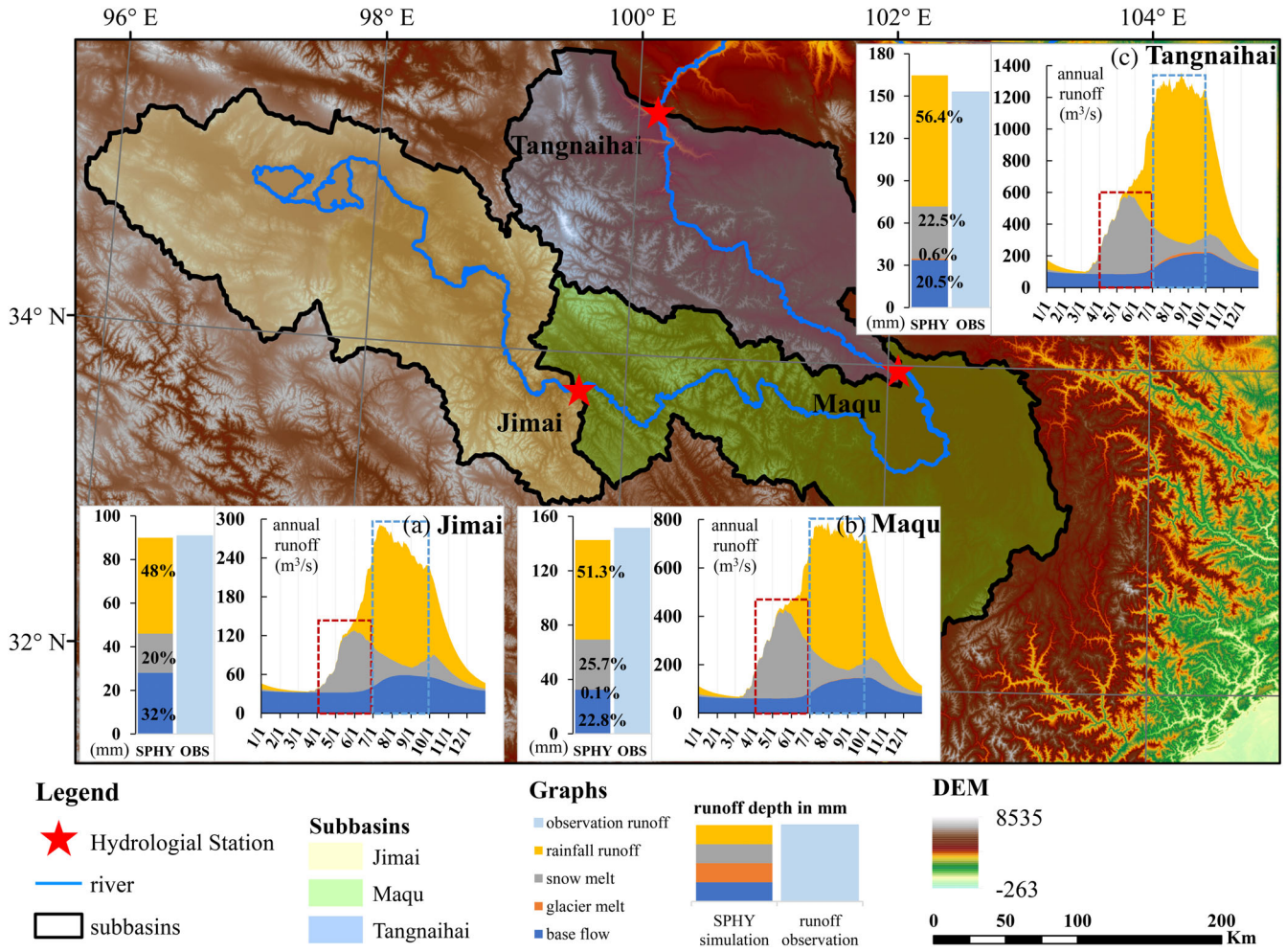

FIGURE 3 Runoff components in the three stations in SYR during 2000–2015: (a) Jimai, (b) Maqu, and (c) Tangnaihai. The red dotted rectangles correspond to the period of spring from April to June. The blue dotted rectangle corresponds to the period of summer from July to September. More details on the seasonal contribution of all runoff components can be found in Table 3. The hydrographs in the right from (a to c) consist of four runoff components: Baseflow (blue), glacier melt flow (orange), snowmelt flow (grey), and rainfall flow (yellow). The bar graphs in the left from (a to c) are the relative contribution in percentage of each runoff component to total runoff and observed runoff depth at each station.

(Figures 3 and 4c). The spatial variation of snowmelt flow can be interpreted by the spatial pattern of precipitation, especially the snowfall (Figure S1). The largest proportion of snowmelt flow at Maqu is consistent with its larger snowfall proportion (Figure S1b), larger amounts of snowfall in winter (Figure S1c), and higher temperature during the snowmelt season from April to June (Figure S2b) than other stations. Rainfall flow accounts for larger proportions in the downstream region (Figure 4d), with the highest contribution at Tangnaihai and the lowest contribution at Jimai because of less precipitation and lower temperature upstream (Figures S1 and S2). Specifically, rainfall flow contributes more than half of the total runoff at the warm-wet downstream stations, contributing 56% at Tangnaihai and 51% at Maqu (Figure 3b, c). The contributions of rainfall flow simulated by SPHY are overall in line with previous estimations based on isotope analysis, ranging from 52% to 53% (Yang et al., 2019). Baseflow makes up a larger share of total runoff at the cold-dry Jimai (32%) and plays a less significant role at the wet-warm downstream stations (only around 20%) (Figures 3 and 4a). This is consistent with previous studies, which found a relatively high contribution of baseflow in regions with a cold and dry climate but less important baseflow in regions with a warm and wet climate (Beck et al., 2013; Cheng et al., 2019). In SYR, the glacier only appears in the downstream region near Tangnaihai (Figure 4b). Glacier coverage is only 0.4% and the glacier-melt flow accounts for 0.6% of the total runoff (Figure 3c).

Furthermore, the dominant runoff component varies among seasons (Figure 3 and Table 3). For instance, in spring, snowmelt flow is the dominant runoff component for the whole SYR, contributing 53%–64% of the spring runoff and playing the most significant role at Maqu (64%). The warmer annual and spring temperatures at downstream stations (Maqu and Tangnaihai, Figure S2a,b) initiate the snowmelt process in March, earlier than that at the upstream Jimai (April, Figure 3). In summer, runoff is dominated by the rainfall flow, which accounts for 68%–75% of the total runoff further downstream. Rainfall flows peak in July at Jimai and Maqu and in August at Tangnaihai.

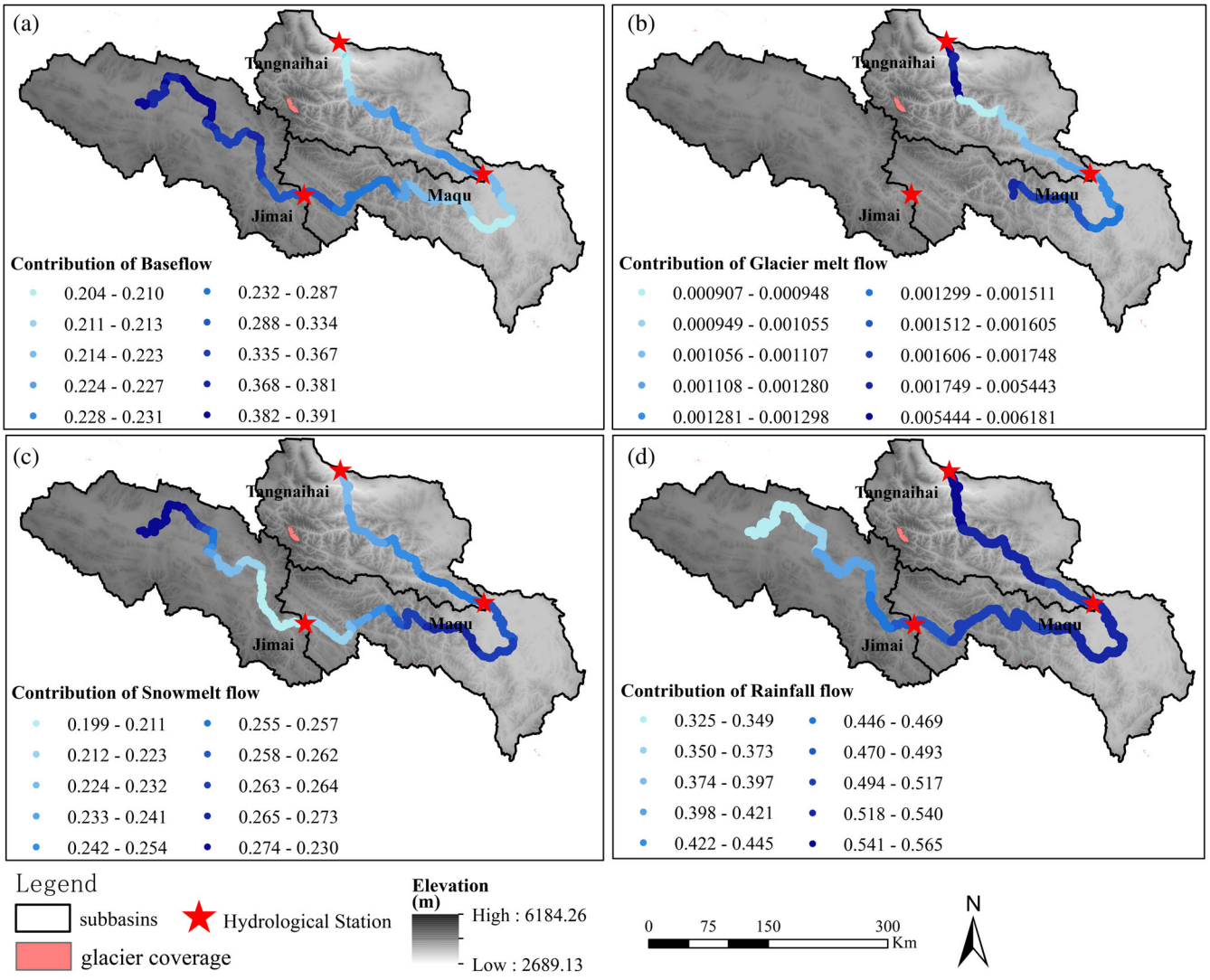

FIGURE 4 Relative contributions of different runoff components to the total runoff in SYR with a spatial resolution of 500 m, namely (a) contribution of baseflow, (b) contribution of glacier melt flow, (c) contribution of snowmelt flow and (d) contribution of rainfall flow.

TABLE 3 Seasonal contribution of runoff components in percentage (%) in three stations from 2000 to 2015. Spring and summer are constrained from April to June and July to September, respectively

Season	Baseflow	Glacier melt flow	Snowmelt flow	Rainfall flow
Jimai				
Spring	23	0	53	24
Summer	21	0	11	68
Maqu				
Spring	14	0.06	64	22
Summer	17	0.17	11	72
Tangnaihai				
Spring	13	0.20	60	27
Summer	15	0.94	9	75

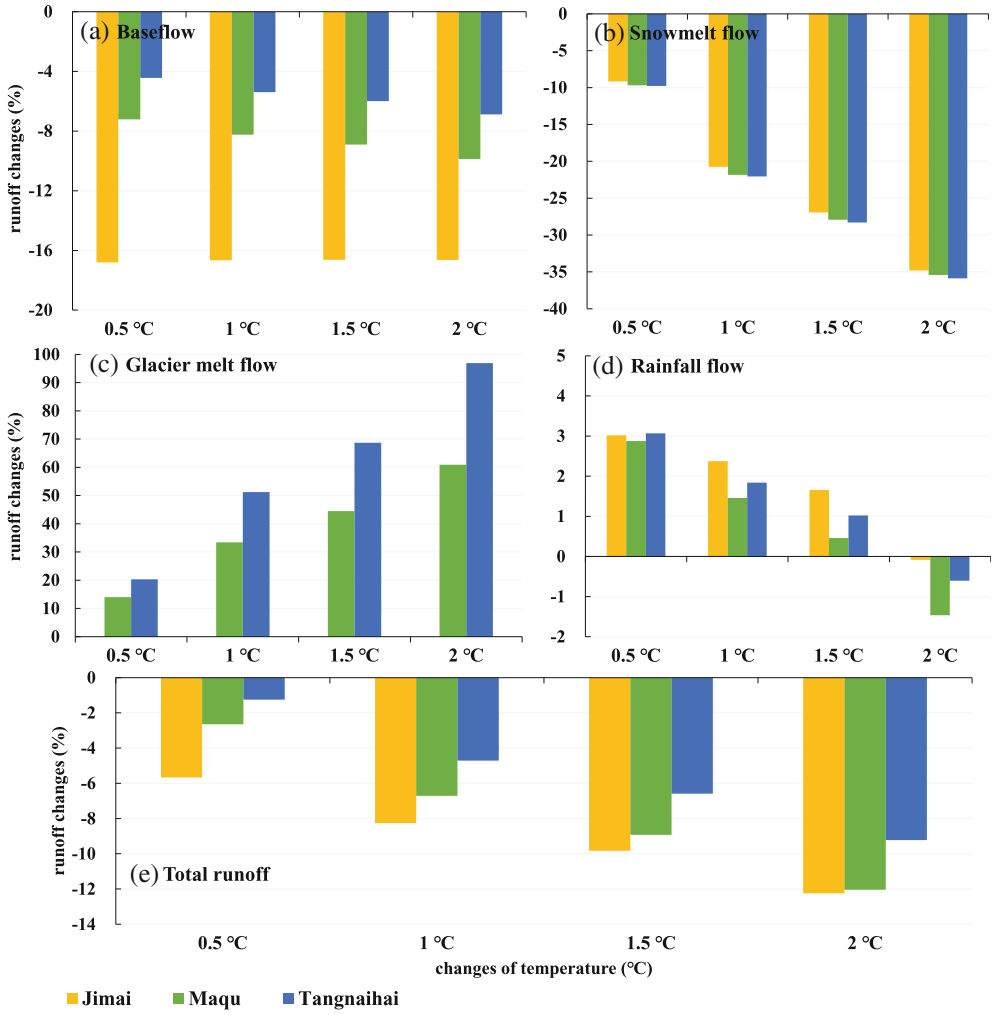

FIGURE 5 Responses of the runoff components to changes in air temperature from 0.5 to 2°C in SYR relative to climate during 2000 to 2015; (a) response of baseflow, (b) response of snowmelt flow, (c) response of rainfall flow, and (d) response of total runoff. The higher bar shows a stronger response. *Y*-axis is the runoff changes in percentage relative to the runoff under the current climate (2000–2015)

Rainfall flows retreat from October at three stations and the recession periods last longer at downstream stations, continuing until March in the following year. Baseflow dominates the runoff from January to March, although baseflow is relatively high from July to November. Glacier meltwater only appears from July to September at downstream stations.

4.2 | Response of runoff components to temperature changes

To analyse the response of runoff components to temperature perturbation in SYR, four future temperature scenarios over 16 years (e.g., net temperature increases of 0.5, 1.0, 1.5, and 2°C relative to the temperature during the period 2000–2015) are simulated. These four hypothetical future temperature scenarios are in line with the projected climate change scenarios generated for the sixth phase of the Climate Model Intercomparison Project (Lalande et al., 2021).

With the temperature increasing from 0.5 to 2°C, the total runoff shows the strongest response at the upstream Jimai (with a reduction from 6% to 12%) and the weakest response at the downstream Tangnaihai (with a reduction from 1% to 9%) (Figure 5e). For different runoff components, glacier-melt flow and snowmelt flow exhibit stronger responses to warming, followed by the response of rainfall flow and baseflow (Figure 5). Glacier-melt flow increases with warming, with a net increase of 97% at Tangnaihai under the 2°C warming scenario (Figure 5c). Snowmelt flow decreases with warming, particularly at the downstream stations. For instance, snowmelt flow decreases by ~10% to ~35% at Maqu and Tangnaihai associated with temperature increases from 0.5 to 2°C (Figure 5b). Baseflow also decreases with warming (Figure 5a). Jimai displays the largest baseflow decline and the decline is weaker at the downstream stations.

The response of rainfall flow to a warming climate is more complicated as it is affected by changes in both precipitation partition (snowfall or rainfall) and evapotranspiration. The response of rainfall flow to temperature increase is nonlinear (Figure 5d). Generally, the increase rate of rainfall flow decreases as the temperature warms. When the temperature increases are constrained within 1.5°C, the rainfall flow increases due to more precipitation in rainfall. The increase in rainfall flow is more significant at the upstream Jimai, increased by 3%–2%. When the temperature increases by 2°C, there is a decline in rainfall flow because of the intensified evapotranspiration. The decline in rainfall flow is evident at the downstream stations (Maqu and Tangnaihai), reduced by 1.5% and 0.60% respectively.

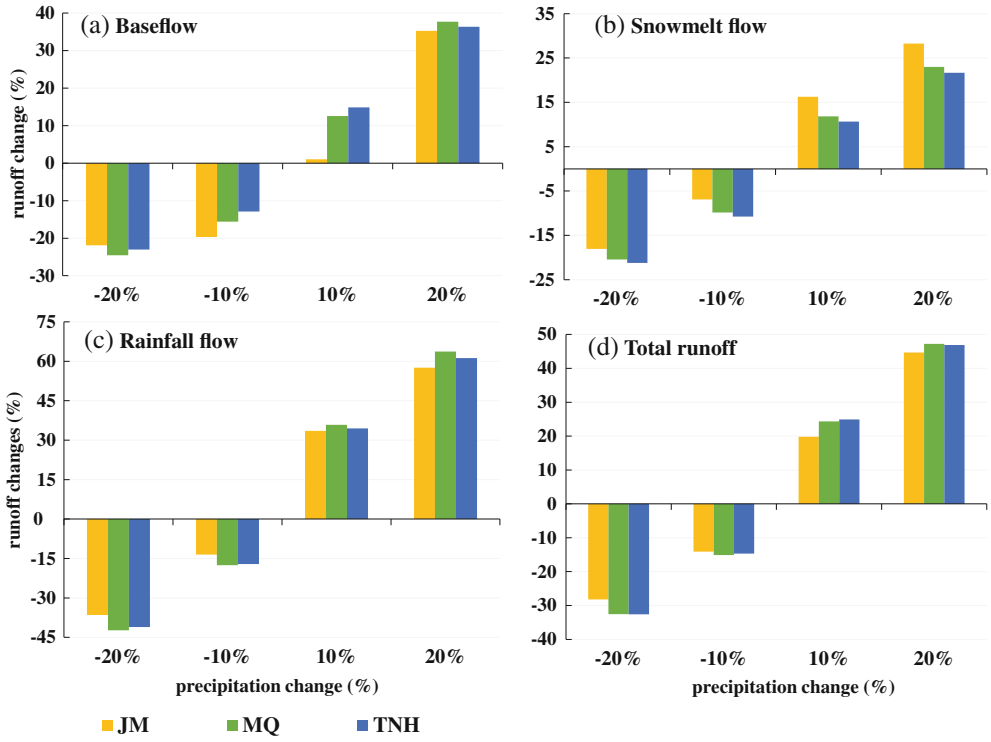

FIGURE 6 Responses of the runoff components to precipitation changes from −20% to 20% in SYR relative to climate during 2000 to 2015; (a) response of baseflow, (b) response of snowmelt flow, (c) response of rainfall flow, and (d) response of total runoff. The higher bar shows a stronger response. *Y*-axis is the runoff changes in percentage relative to the runoff under the current climate (2000–2015)

By comparing the hydrographs under current temperature and a scenario with a 2°C increase in temperature, we find that snowmelt flow initiates earlier in a hydrological year with the snowmelt flow peak advancing by half a month (Figure S3a–c). The early arrival of the peak of snowmelt flow is more obvious at the upstream Jimai, with a net advance of approximately a month (Figure S3a). Furthermore, in spring, snowmelt flow is still the dominant component although its contribution decreases in a warmer climate. The proportions of baseflow and rainfall flow increase. In summer, the dominant rainfall flow makes larger contributions with temperature increase, and the proportions of baseflow and snowmelt flow decrease accordingly.

4.3 | Response of runoff components to precipitation changes

We conduct sensitivity analysis to analyse how various runoff components respond to precipitation changes in SYR. Similar to the temperature sensitivity analysis, four scenarios over 16 years are considered for future precipitation changes (e.g., net precipitation changes of −20%, −10%, 10%, and 20% relative to the historical period 2000–2015).

Although the total runoff increases with higher precipitation for all three stations, there exists spatial variability in the magnitude of responses of total runoff and runoff components (Figure 6). Total runoff at the downstream stations responds more significantly to changes in precipitation than at the upstream station (Figure 6d). Changes in total runoff vary from −33% to 47% at the downstream stations and from −28% to 45% at the upstream Jimai, with precipitation varying from −20% to 20%.

Among different runoff components, the response of rainfall flow to precipitation perturbation is the strongest, followed by baseflow and snowmelt flow (Figure 6). In a wetter climate (precipitation increases by 10%–20%), the upstream station Jimai displays a relatively small increase in rainfall flow (up to 58%) and the increases are larger at the downstream stations (up to 64%); the relatively small response of rainfall flow at Jimai is also found under drying scenarios (precipitation decreases by 10%–20%, Figure 6c). For snowmelt flow, the spatial pattern of its response to precipitation changes is different under wetting and drying scenarios. Specifically, the response magnitude of snowmelt flow is larger at the upstream station under wetting scenarios but is larger at the downstream stations under drying scenarios (Figure 6b). The responses of baseflow to precipitation changes are stronger further downstream, especially under wetting scenarios (Figure 6a).

By comparing the hydrographs under the current climate and a scenario with a 20% change in precipitation, the seasonal response processes of runoff components to wetting (Figure S3d–f) or drying (Figure S3g–i) were depicted. Changes in precipitation can alter the runoff seasonality. There is an asymmetric response of runoff seasonality to precipitation with larger runoff seasonality in a wetter climate and weaker runoff seasonality in a dryer climate. In spring, snowmelt flow takes up larger proportions during drying scenarios, and its proportion declines during wetting scenarios. In summer, the proportion of rainfall flow increases with precipitation, and the proportion of snowmelt flow decreases.

4.4 | Response of runoff components to joint temperature-precipitation changes

According to Hoegh-Guldberg et al. (2019) and Lalande et al. (2021), increases in both temperature and precipitation are the most likely

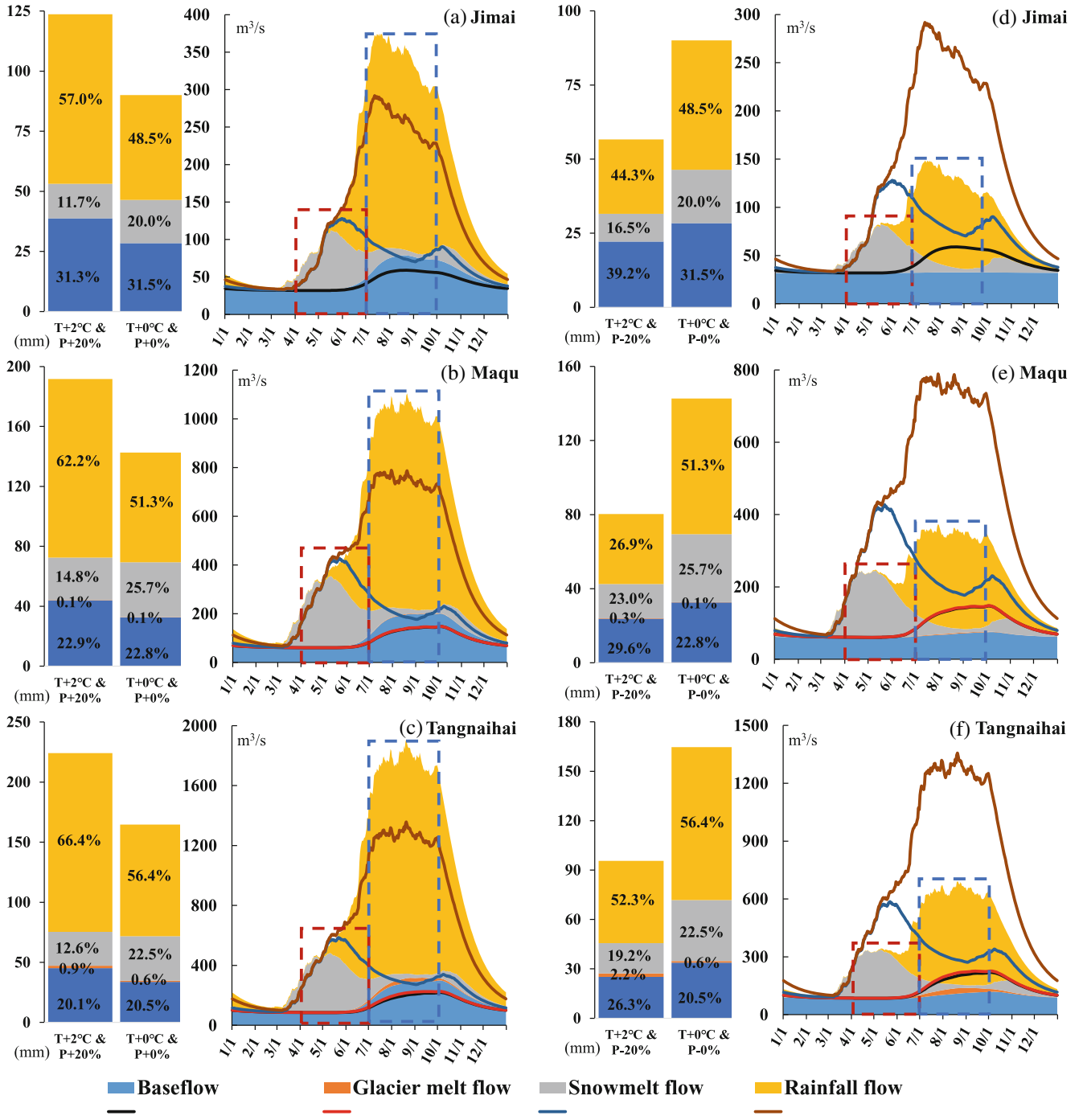

FIGURE 7 Runoff components under a warmer-wetter scenario (temperature increases by 2°C, precipitation increases by 20%) and a warmer-drier (temperature increases by 2°C, precipitation decreases by 20%), relative to the current climate over 2000–2015 in SYR. Left panels (a–c) show the responses of runoff components at Jimai, Maqu, and Tangnaihai under temperature increase by 2°C and precipitation increase by 20%. Right panels (d–f) show the responses of runoff components at Jimai, Maqu, and Tangnaihai under temperature increase by 2°C and precipitation decrease by 20%. The red dotted rectangles correspond to the period of spring from April to June. Blue dotted rectangles correspond to the period of summer from July to September. The hydrographs in the right of Figure 7a–f show the hydrograph under the current climate (drawn by line) and the hydrograph under different scenarios (drawn by filled line). The bar graphs in the left of Figure 7a–f show the relative contribution (in percentage) of each runoff component under different scenarios and the current climate respectively

future climate change scenario in SYR. However, considering the large uncertainty in precipitation projections on the Tibetan Plateau (Huppmann et al., 2018; Lan et al., 2010; Wang et al., 2021), here two future climate change scenarios (e.g. "temperature increase & precipitation increase" and "temperature increase & precipitation decrease") are projected to simulate the responses of runoff components to climate change.

In the scenario with a 2°C temperature increase and a 20% increase in precipitation, the total runoff increases in all three stations, and the seasonal variation of runoff is amplified significantly, with a significant increase in summer flow (Figure 7a–c). The magnitude of the runoff response varies spatially (Figure S4). The increase in total runoff is relatively large at the upstream station Jimai (Figure S4d). Jimai also shows the most significant increase in baseflow (Figure S4a). The reduction of snowmelt flow is stronger at the downstream stations (Figure S4b). Maqu shows the most significant increase in rainfall flow (Figure S4c). When the temperature increases by 2°C and precipitation decreases by 20%, the total runoff decreases at all three stations with significantly flattened hydrographs (Figure 7d–f). There are stronger responses of total runoff and runoff components in the downstream stations under this scenario (Figure S4). The proportion of baseflow rises dramatically, especially at Jimai and Maqu (Figure 7d–e).

5 | DISCUSSION

This study shows that there is a large west–east spatial gradient in hydrological processes and compares the hydrological responses to climatic perturbation between the upstream station (Jimai) and the downstream stations (Maqu and Tangnaihai). The variation may result from the spatial variances in climate (Bronstert et al., 2002; Lutz et al., 2014), land use and land cover (e.g., vegetation cover) (Bronstert et al., 2002; Jordán et al., 2010), permafrost distribution (Qin et al., 2017), and geomorphic features (Li et al., 2019). In this section, we discuss the impacts of climate change on surface flow and the impact of permafrost thaw on baseflow, respectively.

5.1 | Impact of climate change on surface flow

In SYR, the responses of hydrological processes to climate change are different at the upstream and the downstream stations (Figures 5 and 6 and Figure S4). Under the wetting-only scenarios (Figure 6), the increase of total runoff to precipitation changes is higher at the downstream stations than at the upstream station due to the large spatial heterogeneity in precipitation (Figure S1) (Wang et al., 2021) and the stronger influence of rainfall flow downstream (Figure 3). However, under the warming-wetting scenario, the less increase of total runoff was estimated in the downstream stations (Figure 7 and Figure S4). This may be induced by a higher increase in evapotranspiration and a larger reduction in snow meltwater supply in the downstream region in response to atmospheric warming (Kraaijenbrink et al., 2021; Meng et al., 2016).

The changes in rainfall flow in response to temperature variation are nonlinear, especially at the downstream stations (Figure 5d). Rainfall flow increases initially when the temperature rises range from 0.5 to 1.5°C but decreases when the temperature rises to 2°C. The initial increase in rainfall flow with temperature warming mainly arises from the change in precipitation partitioning, accompanied by decreased snowfall and snowmelt flow (Kraaijenbrink et al., 2021). The deceased rainfall flow in the extreme warming scenario can be explained by the spatial pattern of evapotranspiration in SYR (Meng et al., 2016; Qin et al., 2017). At the upstream region, evapotranspiration is relatively weak (Figure S5) due to the cold-dry climate and the widespread bare land (Table 1). By contrast, the downstream region is mainly underlain by grassland and forests (Table 1 and Figure S5), which results in higher evapotranspiration as the climate warms (Calanca et al., 2006). Therefore, high-degree warming (e.g., an increase in temperature by 2°C) causes a net decrease in rainfall flow at the downstream stations, especially at Maqu; such responses are consistent with the widely distributed wetlands and forests near Maqu (Li et al., 2016).

The decline of snowmelt flow with temperature increase is also greater at the downstream stations (Figure 5b). The decreased snowmelt flow is related to the decreased snow accumulation and a transition towards rainfall-dominated precipitation as the climate warms (Duan et al., 2017; Kraaijenbrink et al., 2021). In addition, we show that the snowmelt flow and its flow peak arrive earlier in a hydrological year as the climate warms. The advance of the onset of snowmelt flow is more significant at the upstream station (~15 days) than the downstream stations (~5 days) when the temperature increases by 2°C (Figure S3a–c). Such findings are consistent with earlier studies (Meng et al., 2016; Stone et al., 2002) and have important implications for agriculture management such as the adjustments of sowing dates (Ahmad et al., 2017; Qin et al., 2020). The earlier arrival of snowmelt and the reduced snowmelt flow associated with temperature warming may negatively impact the sustainability of spring irrigation and threaten food security in the entire Yellow River basin (Elias et al., 2015; Qin et al., 2020). This situation would worsen under the warming and drying scenario (Figure 7d–f).

5.2 | Impact of permafrost thaw on baseflow

Baseflow and its contribution to the total runoff will change due to the increase in soil permeability induced by atmospheric warming and permafrost thawing (Terink et al., 2015; Walvoord & Kurylyk, 2016). Over the past decades, half of the permafrost in SYR has degraded into the seasonally frozen ground, with only 17% of the basin area covered by permafrost during the 2000s (Figure S6a–c) (Qin et al., 2017). The substantially warming ground temperatures have been recorded in stations adjacent to SYR over the past decade (Figure S7) (Zhao et al., 2021), associated with the decreased thickness of seasonally frozen ground for the entire SYR (Figure S6d) (Wang, Yang, Qin, et al., 2018). Infiltration of the surface water due to permafrost thaw increases soil moisture, recharges groundwater, and generates baseflow (McCauley et al., 2002; Qin et al., 2017); plays an important role in the hydrological processes at the permafrost-dominated Jimai (Figures 1 and 8b) (Ma et al., 2019; Qin et al., 2017), with the impact weakened further downstream (Figure 9). Our study shows that the spring flow is underestimated at all the three stations (Figures S8-S9), and the late-summer flow is overestimated at Jimai during 2010–2015 (Figure S8), possibly due to the insufficient

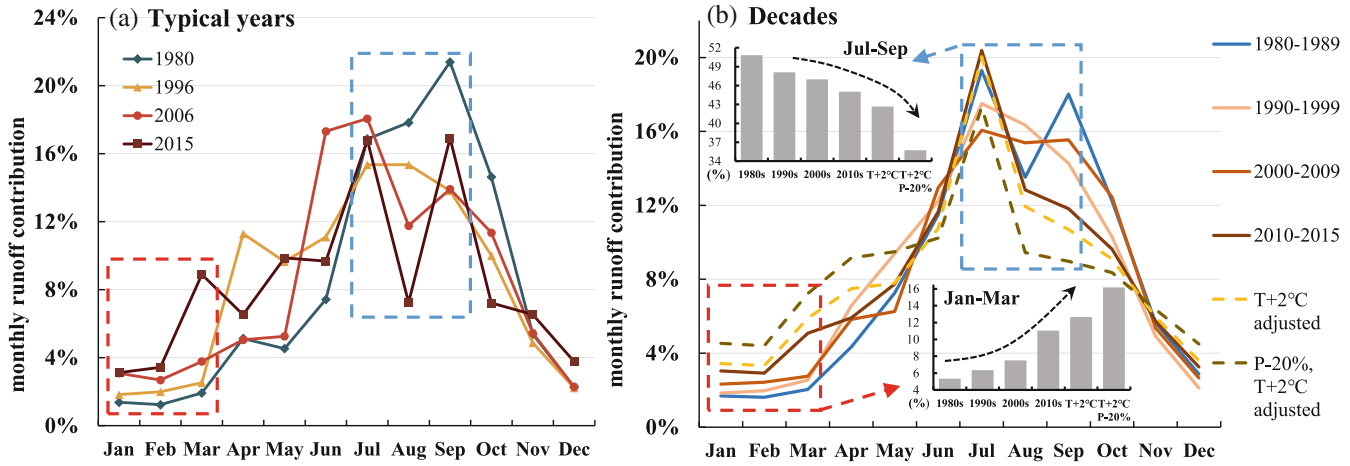

FIGURE 8 Average monthly runoff contribution (%) to the annual runoff at Jimai during (a) typical years from 1980–2015 and (b) decades from 1980–2015 and the warming-drying scenario. The red dotted rectangles refer to the monthly runoff contribution from January to march, when there is almost only baseflow. The blue dotted rectangles refer to the monthly runoff contribution from July to September, when rainfall flow is the dominated. Precipitation, temperature, and average monthly runoff contribution (%) from January–march and July–September of the typical years in (a) can be found in Table S4. The dot lines are the projected monthly runoff contribution (%) by SPHY under the warming scenario (temperature increase by 2°C) and warming-drying scenario (temperature increase by 2°C and precipitation decrease by 20%). The accumulative contributions during the low-flow period (January to march) and high-flow period (July to September) from the 1980s to 2010s are shown in the bar chart in Figure 8b

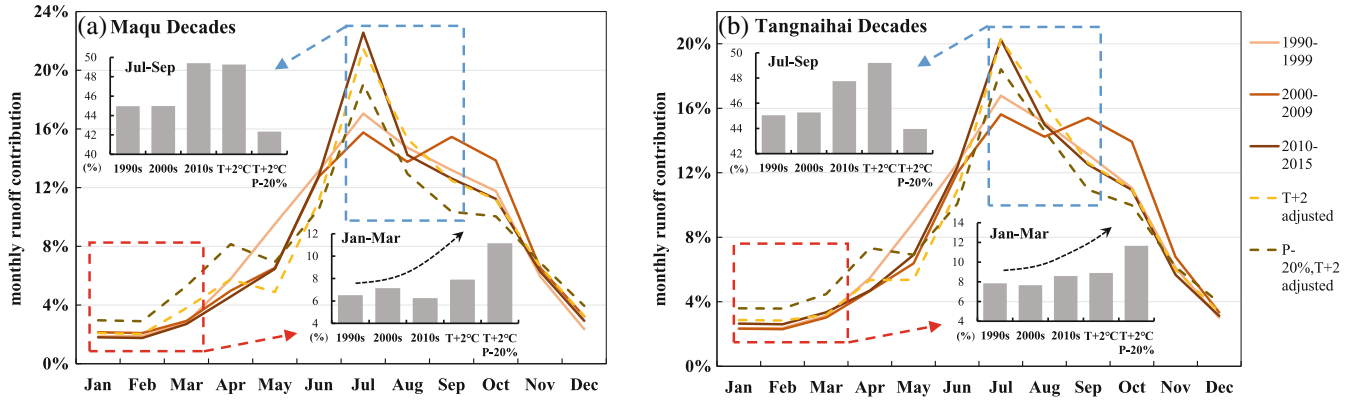

FIGURE 9 Average monthly runoff contribution (%) to the annual runoff at (a) Maqu and (b) Tangnaihai at a decadal scale over 1990–2015 and under the warming and warming-drying scenarios. The red dotted rectangles refer to the monthly runoff contribution from January to march, when baseflow dominates the total runoff. The blue dotted rectangles refer to the monthly runoff contribution from July to September, when rainfall flow is the most important. The dot lines are the projected monthly runoff contribution (%) by SPHY under the warming scenario (an increase in temperature by 2°C) and warming-drying scenario (an increase in temperature by 2°C and a decrease in precipitation by 20%). The accumulative contributions during the low-flow period (January to march) and high-flow period (July to September) from the 1980s to 2010s are shown in the bar chart

representation of permafrost processes in the SPHY model (Khanal et al., 2021).

Here, we analyse the response of baseflow to climate change and permafrost thaw using in-situ runoff observations (Figure 8 and Table 4). The monthly runoff observations and climatic data at Jimai were collected from 1980 to 2015 to capture and verify such permafrost thaw-induced baseflow response. There is almost only baseflow from January to March (e.g., Figure 3) (Cuo et al., 2013), so the observed runoff from January to March is used to represent baseflow. From 1980 to 2015, Jimai experienced significant warming, with the daily maximum temperature rising from −0.05 to 3.27°C (Table 4), indicating an increasing thaw of permafrost during the warming summer (Qin et al., 2017; Wang, Yang, Qin, et al., 2018). Accordingly, the contribution of winter baseflow (January to March) to total runoff increased from 5% to 11% and the contribution of summer flow (July to September) decreased from 51% to 42%, although the annual precipitation increased slightly from 424 to 463 mm. Furthermore, several typical years are chosen to reflect the baseflow responses under different climate change scenarios at Jimai (Figure 8a and Table S3). Specifically, the contribution of winter baseflow to total runoff

TABLE 4 Precipitation, temperature, and average monthly runoff contribution ratio (%) from January to march at Jimai over 1980–2015

Periods	P mm	T_{max} °C	T_{avg} °C	T_{min} °C	Jan–Mar Q %	July–Sep Q %
1980–1989	424	−0.05	−5.29	−11.03	5.34	50.83
1990–1999	392	0.33	−5.08	−11.00	6.36	48.11
2000–2009	458	2.44	−3.97	−10.50	7.50	46.98
2010–2015	463	3.27	−3.22	−9.63	11.05	45.04
2010–2015 with P-20%, T + 2 (adjusted)	370	5.27	−1.22	−7.63	16.16	35.73

Note: P = average annual precipitation. T_{max} = average daily max temperature. T_{avg} = average daily mean temperature, T_{max} = average daily min temperature, Jan–Mar Q = average monthly runoff contribution ratio (%) from January to march, July–Sep Q = average monthly runoff contribution ratio (%) from July to September.

TABLE 5 Precipitation, temperature, and average monthly runoff contribution ratio (%) from January to march at Maqu and Tangnaihai over 1990–2015

Periods	P mm	T_{max} °C	T_{avg} °C	T_{min} °C	Jan–Mar Q %	July–Sep Q %
Maqu						
1990–1999	643	5.34	−0.63	−6.51	6.52	44.96
2000–2009	643	7.03	0.28	−6.31	7.15	44.97
2010–2015	698	7.61	0.65	−6.02	6.25	49.40
2010–2015 with P-20%, T + 2 (adjusted)	558	0.61	2.65	−4.02	11.14	42.34
Tangnaihai						
1990–1999	485	2.97	−2.94	−9.03	7.84	45.05
2000–2009	548	4.79	−1.92	−8.56	7.65	45.27
2010–2015	567	5.20	−1.49	−8.02	8.59	47.76
2010–2015 with P-20%, T + 2 (adjusted)	454	7.20	1.49	−6.02	11.65	43.96

Note: P = average annual precipitation, T_{max} = average daily max temperature, T_{avg} = average daily mean temperature, T_{max} = average daily min temperature, Jan–Mar Q = average monthly runoff contribution ratio (%) from January to March, July–Sep Q = average monthly runoff contribution ratio (%) from July to September.

doubled (10%) in the warmer and wetter year of 2006 compared with the year 1980 (5%). The contribution of winter baseflow increased more significantly (almost tripled) in the warmer and dryer year of 2015 (15%) compared with the year 1996 (6%). Based on the bias analysis of the monthly runoff contribution between observations and simulations (Text S2) at Jimai from 2010 to 2015, the monthly runoff contribution ratios under different scenarios are reassessed (Figure S8). After reassessment, the winter baseflow would contribute to 13% of total runoff when the temperature increases by 2°C, and the ratio of winter baseflow would increase to 16% under the warming and drying scenario (Figure 8b). Yet, runoff seasonality at two downstream stations is less impacted by permafrost thaw but more regulated by precipitation and human activities (Figure 9). The contributions of winter baseflow to total runoff at two downstream stations do not show a concomitant trend with temperate over the past three decades; the contributions of summer flow are largely controlled by precipitation, with a concomitant pattern (Table 5). Runoff seasonality at Tangnaihai is also likely complicated by human activities due to more small hydropower dams and reservoirs being in operation after 2000 (Ma et al., 2019).

With permafrost thawing, surface flow infiltration and the baseflow contribution will increase at the upstream part of SYR (Table 4). The contribution of rainfall flow and snowmelt flow in warmer seasons would be reduced due to more surface water recharging the groundwater, which leads to less available surface water (Qin et al., 2017; Walvoord et al., 2012). Importantly, the runoff regime will likely transition from a surface water-dominated system towards a groundwater-dominated system, especially at the permafrost-dominated Jimai (Figure 8). This type of shift in runoff regime has also been reported in other large-scale studies in the Arctic (Frey & McClelland, 2009; Walvoord & Kurylyk, 2016).

6 | CONCLUSIONS

This study has distinguished the different runoff components and interpreted their responses to changes in air temperature and precipitation at three hydrological stations (Jimai, Maqu, and Tangnaihai) in the source-region of the Yellow River (SYR), based on a fully-

distributed high-resolution cryosphere-hydrology model and multi-decadal runoff observations. Results show that rainfall flow is the dominant runoff component in SYR, especially in the downstream stations, contributing 51% and 56% in Maqu and Tangnaihai respectively. Snowmelt flow ranks secondly among the four runoff components at Maqu (26%) and Tangnaihai (23%) and thirdly at Jimai (20%). Baseflow is more important at the upstream station (32%; Jimai) than at the downstream stations (21%–23%; Maqu and Tangnaihai). Glacier melt from Anyê Maqên and Bayankala Mountains only exists at the downstream stations with negligible contributions (<1%).

The responses of multiple hydrologic processes to changes in air temperature and precipitation vary between the upstream station and the downstream stations. As increases in air temperature and precipitation (the most likely future climate change scenario in SYR) (Lalande et al., 2021), the warm-wet downstream stations show a smaller increase in the total runoff than the cold-dry upstream station because of a larger reduction in snowmelt flow and higher evapotranspiration-induced water loss. Rainfall flows display a non-linear response to temperature increase, with an initially increased rainfall flow when the temperature increase is less than 1.5°C and a decreased rainfall flow (especially at the downstream stations) when the temperature increase exceeds 2°C. Snowmelt flow decreases with temperature increase, with higher declines at downstream stations than at the upstream station. Snowmelt flow starts earlier when temperature increases, and this phenomenon is more obvious in the upstream region. Furthermore, with permafrost thawing, the contribution of baseflow to the total runoff would increase and this might lead to the shift from a surface water-dominated system towards a groundwater-dominated system in the upstream permafrost-dominated region.

Given the predominant role of freshwater supply from SYR to the entire Yellow River, the findings have important implications for downstream hydropower reservoirs, agricultural irrigation, and thus food-energy security. The decreased snowmelt flow with temperature warming indicates the weakened seasonal buffering role of snow meltwater; the decreased surface flow due to permafrost thaw renders the increasingly important role of groundwater storage in the water supply. These hydrological shifts provide insights for policymakers to improve the management of local water resources (e.g., enhancing basin reservoir storage capacity) and plan strategies (e.g., optimizing irrigation schedules and irrigation systems) to adapt to future changes in climate and hydrological regimes. However, this research does not investigate the impacts of human activities (e.g., dam construction and land-use change) on streamflow in SYR. Since 2000, there has been an increase in human activities in the downstream region. For example, some small dams have been built near Tangnaihai for irrigation and hydropower generation, including Pandoh, Moduo, Dangcun, and Gadu dams. Thus, the hydrological influences of these human activities need to be considered in future studies using models with more accurate representations of these anthropogenic interventions (He et al., 2017; Yang et al., 2020).

ACKNOWLEDGEMENT

This study is supported by the Ministry of Education of Singapore (R-109-000-273-112; R-109-000-227-115; NUS President Graduate Fellowship). D. Li is supported by the Cuomo Foundation and IPCC scholarship award for early-career scientists. The authors acknowledge the valuable comments provided by Dr. Xiaogang He.

DATA AVAILABILITY STATEMENT

Discharge data was sourced and available from the Qinghai Hydrology Bureau and Yellow River Conservancy Commission of the Ministry of Water Resources (http://www.yrcc.gov.cn/). Precipitation and air temperature data were sourced from the China Meteorological Forcing Dataset (CMFD, https://data.tpdc.ac.cn/en/data/8028b944-daaa-4511-8769-965612652c49/). Elevation data was downloaded from Resource and Environment Science and Data Center (http://www.resdc.cn/data). Land cover data was derived from GlobCover Land Cover Map developed by the European Space Agency (http://due.esrin.esa.int/page_globcover.php). Soil types were derived from the China soil map (http://westdc.westgis.ac.cn/zh-hans/data/). Physical parameters of different soil types were derived from the HiHydroSoil database (http://www.sphy.nl/). Glacier coverage was derived from Randolph Glacier Inventory (RGI V6.0, https://www.glims.org/RGI/rgi60_dl.html).

ORCID

Ting Zhang https://orcid.org/0000-0003-4975-0200
Dongfeng Li https://orcid.org/0000-0003-0119-5797
Xixi Lu https://orcid.org/0000-0002-2528-4631

REFERENCES

Ahmad, S., Abbas, Q., Abbas, G., Fatima, Z., Atique Ur, R., Naz, S., … Hasanuzzaman, M. (2017). Quantification of climate warming and crop management impacts on cotton phenology. *Plants (Basel)*, *6*(1), 7. https://doi.org/10.3390/plants6010007

Beck, H. E., van Dijk, A. I. J. M., Miralles, D. G., de Jeu, R. A. M., Bruijnzeel, L. A., McVicar, T. R., & Schellekens, J. (2013). Global patterns in base flow index and recession based on streamflow observations from 3394 catchments. *Water Resources Research*, *49*(12), 7843–7863. https://doi.org/10.1002/2013WR013918

Bronstert, A., Niehoff, D., & Bürger, G. (2002). Effects of climate and land-use change on storm runoff generation: Present knowledge and modelling capabilities. *Hydrological Processes*, *16*(2), 509–529. https://doi.org/10.1002/hyp.326

Cai, X., & Rosegrant, M. W. (2004). Optional water development strategies for the Yellow River Basin: Balancing agricultural and ecological water demands. *Water Resources Research*, *40*(8), W08S04. https://doi.org/10.1029/2003wr002488

Calanca, P., Roesch, A., Jasper, K., & Wild, M. (2006). Global warming and the summertime evapotranspiration regime of the alpine region. *Climatic Change*, *79*(1), 65–78. https://doi.org/10.1007/s10584-006-9103-9

Cheng, Y., Ogden, F. L., & Zhu, J. (2019). Characterization of sudden and sustained base flow jump hydrologic behaviour in the humid seasonal tropics of the Panama Canal watershed. *Hydrological Processes*, *34*(3), 569–582. https://doi.org/10.1002/hyp.13604

Cuo, L., Zhang, Y., Gao, Y., Hao, Z., & Cairang, L. (2013). The impacts of climate change and land cover/use transition on the hydrology in the upper Yellow River Basin, China. *Journal of Hydrology*, *502*, 37–52. https://doi.org/10.1016/j.jhydrol.2013.08.003

Duan, W., He, B., Takara, K., Luo, P., Nover, D., & Hu, M. (2017). Impacts of climate change on the hydro-climatology of the upper Ishikari river basin, Japan. *Environmental Earth Sciences*, *76*(14), 1–16. https://doi.org/10.1007/s12665-017-6805-4

Duan, W., Zou, S., Chen, Y., Nover, D., Fang, G., & Wang, Y. (2020). Sustainable water management for cross-border resources: The Balkhash Lake Basin of Central Asia, 1931–2015. *Journal of Cleaner Production*, *263*, 121614. https://doi.org/10.1016/j.jclepro.2020.121614

Elias, E. H., Rango, A., Steele, C. M., Mejia, J. F., & Smith, R. (2015). Assessing climate change impacts on water availability of snowmelt-dominated basins of the upper Rio Grande basin. *Journal of Hydrology: Regional Studies*, *3*, 525–546. https://doi.org/10.1016/j.ejrh.2015.04.004

Foglia, L., Hill, M. C., Mehl, S. W., & Burlando, P. (2009). Sensitivity analysis, calibration, and testing of a distributed hydrological model using error-based weighting and one objective function. *Water Resources Research*, *45*(6), W06427. https://doi.org/10.1029/2008wr007255

Frey, K. E., & McClelland, J. W. (2009). Impacts of permafrost degradation on arctic river biogeochemistry. *Hydrological Processes*, *23*(1), 169–182. https://doi.org/10.1002/hyp.7196

Han, Z., Long, D., Fang, Y., Hou, A., & Hong, Y. (2019). Impacts of climate change and human activities on the flow regime of the dammed Lancang River in Southwest China. *Journal of Hydrology*, *570*, 96–105. https://doi.org/10.1016/j.jhydrol.2018.12.048

He, J., Yang, K., Tang, W., Lu, H., Qin, J., Chen, Y., & Li, X. (2020). The first high-resolution meteorological forcing dataset for land process studies over China. *Sci Data*, *7*(1), 25. https://doi.org/10.1038/s41597-020-0369-y

He, X., Wada, Y., Wanders, N., & Sheffield, J. (2017). Intensification of hydrological drought in California by human water management. *Geophysical Research Letters*, *44*(4), 1777–1785. https://doi.org/10.1002/2016gl071665

Hoegh-Guldberg, O., Jacob, D., Taylor, M., Guillén Bolaños, T., Bindi, M., Brown, S., … Zhou, G. (2019). The human imperative of stabilizing global climate change at 1.5°C. *Science*, *365*(6459), eaaw6974. https://doi.org/10.1126/science.aaw6974

Hu, Y., Maskey, S., & Uhlenbrook, S. (2011). Trends in temperature and rainfall extremes in the Yellow River source region, China. *Climatic Change*, *110*(1–2), 403–429. https://doi.org/10.1007/s10584-011-0056-2

Hu, Y., Maskey, S., Uhlenbrook, S., & Zhao, H. (2011). Streamflow trends and climate linkages in the source region of the Yellow River, China. *Hydrological Processes*, *25*(22), 3399–3411. https://doi.org/10.1002/hyp.8069

Huang, Q., Qin, G., Zhang, Y., Tang, Q., Liu, C., Xia, J., … Post, D. (2020). Using remote sensing data-based hydrological model calibrations for predicting runoff in ungauged or poorly gauged catchments. *Water Resources Research*, *56*(8), e2020WR028205. https://doi.org/10.1029/2020wr028205

Huppmann, D., Rogelj, J., Kriegler, E., Krey, V., & Riahi, K. (2018). A new scenario resource for integrated 1.5 °C research. *Nature Climate Change*, *8*(12), 1027–1030. https://doi.org/10.1038/s41558-018-0317-4

Immerzeel, W. W., Lutz, A. F., Andrade, M., Bahl, A., Biemans, H., Bolch, T., … Baillie, J. E. M. (2020). Importance and vulnerability of the world's water towers. *Nature*, *577*(7790), 364–369. https://doi.org/10.1038/s41586-019-1822-y

Immerzeel, W. W., Pellicciotti, F., & Bierkens, M. F. P. (2013). Rising river flows throughout the twenty-first century in two Himalayan glacierized watersheds. *Nature Geoscience*, *6*(9), 742–745. https://doi.org/10.1038/ngeo1896

Immerzeel, W. W., van Beek, L. P., & Bierkens, M. F. (2010). Climate change will affect the Asian water towers. *Science*, *328*(5984), 1382–1385. https://doi.org/10.1126/science.1183188

Jin, J., Wang, G., Zhang, J., Yang, Q., Liu, C., Liu, Y., … He, R. (2018). Impacts of climate change on hydrology in the Yellow River source region, China. *Journal of Water and Climate Change*, *11*(3), 916–930. https://doi.org/10.2166/wcc.2018.085

Jordán, A., Zavala, L. M., & Gil, J. (2010). Effects of mulching on soil physical properties and runoff under semi-arid conditions in southern Spain. *Catena*, *81*(1), 77–85. https://doi.org/10.1016/j.catena.2010.01.007

Khanal, S., Lutz, A. F., Kraaijenbrink, P. D. A., van den Hurk, B., Yao, T., & Immerzeel, W. W. (2021). Variable 21st century climate change response for Rivers in High Mountain Asia at seasonal to decadal time scales. *Water Resources Research*, *57*(5), e2020WR029266. https://doi.org/10.1029/2020wr029266

Kraaijenbrink, P. D. A., Stigter, E. E., Yao, T., & Immerzeel, W. W. (2021). Climate change decisive for Asia's snow meltwater supply. *Nature Climate Change*, *11*(7), 591–597. https://doi.org/10.1038/s41558-021-01074-x

Lalande, M., Ménégoz, M., Krinner, G., Naegeli, K., & Wunderle, S. (2021). Climate change in the High Mountain Asia in CMIP6. *Earth System Dynamics*, *12*(4), 1061–1098. https://doi.org/10.5194/esd-12-1061-2021

Lan, Y., Zhao, G., Zhang, Y., Wen, J., Hu, X., Liu, J., … Ma, J. (2010). Response of runoff in the headwater region of the Yellow River to climate change and its sensitivity analysis. *Journal of Geographical Sciences*, *20*(6), 848–860. https://doi.org/10.1007/s11442-010-0815-4

Li, D., Li, Z., Zhou, Y., & Lu, X. (2020). Substantial increases in the water and sediment fluxes in the headwater region of the Tibetan plateau in response to global warming. *Geophysical Research Letters*, *47*(11), e2020GL087745. https://doi.org/10.1029/2020GL087745

Li, D., Lu, X., Overeem, I., Walling, D. E., Syvitski, J., Kettner, A. J., … Zhang, T. (2021). Exceptional increases in fluvial sediment fluxes in a warmer and wetter High Mountain Asia. *Science*, *374*(6567), 599–603. https://doi.org/10.1126/science.abi9649

Li, D., Lu, X. X., Chen, L., & Wasson, R. J. (2019). Downstream geomorphic impact of the three gorges dam: With special reference to the channel bars in the middle Yangtze River. *Earth Surface Processes and Landforms*, *44*(13), 2660–2670. https://doi.org/10.1002/esp.4691

Li, X., Xue, Z., & Gao, J. (2016). Dynamic changes of plateau wetlands in Madou County, the Yellow River source zone of China: 1990–2013. *Wetlands*, *36*(2), 299–310. https://doi.org/10.1007/s13157-016-0739-6

Lu, W., Wang, W., Shao, Q., Yu, Z., Hao, Z., Xing, W., … Li, J. (2018). Hydrological projections of future climate change over the source region of Yellow River and Yangtze River in the Tibetan plateau: A comprehensive assessment by coupling RegCM4 and VIC model. *Hydrological Processes*, *32*(13), 2096–2117. https://doi.org/10.1002/hyp.13145

Lutz, A. F., Immerzeel, W. W., Shrestha, A. B., & Bierkens, M. F. P. (2014). Consistent increase in high Asia's runoff due to increasing glacier melt and precipitation. *Nature Climate Change*, *4*(7), 587–592. https://doi.org/10.1038/nclimate2237

Ma, Q., Jin, H.-J., Bense, V. F., Luo, D.-L., Marchenko, S. S., Harris, S. A., & Lan, Y.-C. (2019). Impacts of degrading permafrost on streamflow in the source area of Yellow River on the Qinghai-Tibet plateau, China. *Advances in Climate Change Research*, *10*(4), 225–239. https://doi.org/10.1016/j.accre.2020.02.001

McCauley, C. A., White, D. M., Lilly, M. R., & Nyman, D. M. (2002). A comparison of hydraulic conductivities, permeabilities and infiltration rates in frozen and unfrozen soils. *Cold Regions Science and Technology*, *34*(2), 117–125. https://doi.org/10.1016/S0165-232X(01)00064-7

Meng, F., Su, F., Yang, D., Tong, K., & Hao, Z. (2016). Impacts of recent climate change on the hydrology in the source region of the Yellow River basin. *Journal of Hydrology: Regional Studies*, *6*, 66–81. https://doi.org/10.1016/j.ejrh.2016.03.003

Moriasi, D. N., Arnold, J. G., Van Liew, M. W., Bingner, R. L., Harmel, R. D., & Veith, T. L. (2007). Model evaluation guidelines for systematic quantification of accuracy in watershed simulations. *Transactions of the ASABE*, *50*(3), 885–900. https://doi.org/10.13031/2013.23153

Nash, J. E., & Sutcliffe, J. V. (1970). River flow forecasting through conceptual models part I—A discussion of principles. *Journal of Hydrology*, *10*(3), 282–290. https://doi.org/10.1016/0022-1694(70)90255-6

Pfeffer, W. T., Arendt, A. A., Bliss, A., Bolch, T., Cogley, J. G., Gardner, A. S., … Sharp, M. J. (2014). The Randolph glacier inventory: A globally complete inventory of glaciers. *Journal of Glaciology*, *60*(221), 537–552. https://doi.org/10.3189/2014JoG13J176

Pritchard, H. D. (2019). Asia's shrinking glaciers protect large populations from drought stress. *Nature*, *569*(7758), 649–654. https://doi.org/10.1038/s41586-019-1240-1

Qin, Y., Abatzoglou, J. T., Siebert, S., Huning, L. S., AghaKouchak, A., Mankin, J. S., … Mueller, N. D. (2020). Agricultural risks from changing snowmelt. *Nature Climate Change*, *10*(5), 459–465. https://doi.org/10.1038/s41558-020-0746-8

Qin, Y., Yang, D., Gao, B., Wang, T., Chen, J., Chen, Y., … Zheng, G. (2017). Impacts of climate warming on the frozen ground and eco-hydrology in the Yellow River source region, China. *Sci Total Environ*, *605-606*, 830–841. https://doi.org/10.1016/j.scitotenv.2017.06.188

Song, X., Yang, G., Yan, C., Duan, H., Liu, G., & Zhu, Y. (2009). Driving forces behind land use and cover change in the Qinghai-Tibetan plateau: A case study of the source region of the Yellow River, Qinghai Province, China. *Environmental Earth Sciences*, *59*(4), 793–801. https://doi.org/10.1007/s12665-009-0075-8

Stone, R. S., Dutton, E. G., Harris, J. M., & Longenecker, D. (2002). Earlier spring snowmelt in northern Alaska as an indicator of climate change. *Journal of Geophysical Research: Atmospheres*, *107*(D10), ACL 10-11–ACL 10-13. https://doi.org/10.1029/2000jd000286

Terink, W., Lutz, A. F., Simons, G. W. H., Immerzeel, W. W., & Droogers, P. (2015). SPHY v2.0: Spatial processes in hydrology. *Geoscientific Model Development*, *8*(7), 2009–2034. https://doi.org/10.5194/gmd-8-2009-2015

Tiel, M., Stahl, K., Freudiger, D., & Seibert, J. (2020). Glacio-hydrological model calibration and evaluation. *WIREs Water*, *7*, e1483. https://doi.org/10.1002/wat2.1483

Walvoord, M. A., & Kurylyk, B. L. (2016). Hydrologic impacts of thawing permafrost-a review. *Vadose Zone Journal*, *15*(6), 1–20. https://doi.org/10.2136/vzj2016.01.0010

Walvoord, M. A., Voss, C. I., & Wellman, T. P. (2012). Influence of permafrost distribution on groundwater flow in the context of climate-driven permafrost thaw: Example from Yukon Flats Basin, Alaska, United States. *Water Resources Research*, *48*(7), W07524. https://doi.org/10.1029/2011WR011595

Wang, T., Yang, D., Qin, Y., Wang, Y., Chen, Y., Gao, B., & Yang, H. (2018). Historical and future changes of frozen ground in the upper Yellow River Basin. *Global and Planetary Change*, *162*, 199–211. https://doi.org/10.1016/j.gloplacha.2018.01.009

Wang, T., Yang, H., Yang, D., Qin, Y., & Wang, Y. (2018). Quantifying the streamflow response to frozen ground degradation in the source region of the Yellow River within the Budyko framework. *Journal of Hydrology*, *558*, 301–313. https://doi.org/10.1016/j.jhydrol.2018.01.050

Wang, T., Zhao, Y., Xu, C., Ciais, P., Liu, D., Yang, H., … Yao, T. (2021). Atmospheric dynamic constraints on Tibetan plateau freshwater under Paris climate targets. *Nature Climate Change*, *11*(3), 219–225. https://doi.org/10.1038/s41558-020-00974-8

Yang, J., Huang, M., & Zhai, P. (2021). Performance of the CRA-40/land, CMFD, and ERA-interim datasets in reflecting changes in surface air temperature over the Tibetan plateau. *Journal of Meteorological Research*, *35*(4), 663–672. https://doi.org/10.1007/s13351-021-0196-x

Yang, X., Zhang, M., He, X., Ren, L., Pan, M., Yu, X., … Sheffield, J. (2020). Contrasting influences of human activities on hydrological drought regimes over China based on high-resolution simulations. *Water Resources Research*, *56*(6), e2019WR025843. https://doi.org/10.1029/2019wr025843

Yang, Y., Wu, Q., Jin, H., Wang, Q., Huang, Y., Luo, D., … Jin, X. (2019). Delineating the hydrological processes and hydraulic connectivities under permafrost degradation on northeastern Qinghai-Tibet plateau, China. *Journal of Hydrology*, *569*, 359–372. https://doi.org/10.1016/j.jhydrol.2018.11.068

Yuan, F., Wang, B., Shi, C., Cui, W., Zhao, C., Liu, Y., … Yang, X. (2018). Evaluation of hydrological utility of IMERG final run V05 and TMPA 3B42V7 satellite precipitation products in the Yellow River source region, China. *Journal of Hydrology*, *567*, 696–711. https://doi.org/10.1016/j.jhydrol.2018.06.045

Yue, F.-J., Li, S.-L., Liu, C.-Q., Zhao, Z.-Q., & Ding, H. (2017). Tracing nitrate sources with dual isotopes and long term monitoring of nitrogen species in the Yellow River, China. *Scientific Reports*, *7*(1), 8537. https://doi.org/10.1038/s41598-017-08756-7

Zhang, X., Srinivasan, R., Debele, B., & Hao, F. (2008). Runoff simulation of the headwaters of the Yellow River using the SWAT model with three snowmelt Algorithms1. *Journal of the American Water Resources Association*, *44*(1), 48–61. https://doi.org/10.1111/j.1752-1688.2007.00137.x

Zhao, L., Zou, D., Hu, G., Wu, T., Du, E., Liu, G., … Cheng, G. (2021). A synthesis dataset of permafrost thermal state for the Qinghai–Tibet (Xizang) plateau, China. *Earth System Science Data*, *13*(8), 4207–4218. https://doi.org/10.5194/essd-13-4207-2021

Zheng, H., Zhang, L., Zhu, R., Liu, C., Sato, Y., & Fukushima, Y. (2009). Responses of streamflow to climate and land surface change in the headwaters of the Yellow River Basin. *Water Resources Research*, *45*(7), W00A19. https://doi.org/10.1029/2007wr006665

Zheng, Y., Huang, Y., Zhou, S., Wang, K., & Wang, G. (2018). Effect partition of climate and catchment changes on runoff variation at the headwater region of the Yellow River based on the Budyko complementary relationship. *Science of the Total Environment*, *643*, 1166–1177. https://doi.org/10.1016/j.scitotenv.2018.06.195

Zhou, D., & Huang, R. (2012). Response of water budget to recent climatic changes in the source region of the Yellow River. *Chinese Science Bulletin*, *57*(17), 2155–2162. https://doi.org/10.1007/s11434-012-5041-2

Zhou, J., Wang, L., Zhang, Y., Guo, Y., Li, X., & Liu, W. (2015). Exploring the water storage changes in the largest lake (Selin co) over the Tibetan plateau during 2003–2012 from a basin-wide hydrological modeling. *Water Resources Research*, *51*(10), 8060–8086. https://doi.org/10.1002/2014wr015846

SUPPORTING INFORMATION

Additional supporting information can be found online in the Supporting Information section at the end of this article.

How to cite this article: Zhang, T., Li, D., & Lu, X. (2022). Response of runoff components to climate change in the source-region of the Yellow River on the Tibetan plateau. *Hydrological Processes*, *36*(6), e14633. https://doi.org/10.1002/hyp.14633